Draft version October 21, 2016
Preprint typeset using LaTeX style emulateapj v. 5/2/11

arXiv:1610.06180v1 [astro-ph.SR] 19 Oct 2016

HUBBLE TARANTULA TREASURY PROJECT V. THE STAR CLUSTER HODGE 301: THE OLD FACE OF 30 DORADUS

M. Cignoni[2,3,4], E. Sabbi[3], R. P. van der Marel[3], D. J. Lennon[5], M. Tosi[6],E. K. Grebel[7], Gallagher, J. S., III[8], A. Aloisi[3],G. de Marchi[9],D. A. Gouliermis[10,11], S. Larsen[12], N. Panagia[3,13,14], L. J. Smith[15]

Draft version October 21, 2016

ABSTRACT

Based on color-magnitude diagrams (CMDs) from the Hubble Space Telescope Hubble Tarantula Treasury Project (HTTP) survey, we present the star formation history (SFH) of Hodge 301, the oldest star cluster in the Tarantula Nebula. The HTTP photometry extends faint enough to reach, for the first time, the cluster pre-main sequence (PMS) turn-on, where the PMS joins the main sequence. Using the location of this feature, along with synthetic CMDs generated with the latest PARSEC models, we find that Hodge 301 is older than previously thought, with an age between 26.5 and 31.5 Myr. From this age, we also estimate that between 38 and 61 supernovae Type-II exploded in the region. The same age is derived from the main sequence turn-off, whereas the age derived from the post-main sequence stars is younger and between 20 and 25 Myr. Other relevant parameters are a total stellar mass of $\approx 8800 \pm 800 M_{\odot}$ and average reddening $E(B-V) \approx 0.22 - 0.24$ mag, with a differential reddening $\delta E(B-V) \approx 0.04$ mag.

Subject headings: stellar evolution - star forming region: individual, 30 Doradus, galaxies: stellar content

1. INTRODUCTION

The closest starburst region, 30 Doradus in the Large Magellanic Cloud (LMC), allows one to study the star formation (SF) process on a variety of scales, from the dense cluster R 136, possibly a newborn globular cluster, via the massive star-forming region NGC 2070, the "old" (20 to 25 Myr, Grebel & Chu 2000) populous cluster Hodge 301, to the many diffuse star-forming regions like NGC 2060. Deciphering the history of 30 Doradus is therefore a unique opportunity to understand how star formation originates and propagates. In previous work (Cignoni et al. 2015) we studied NGC 2070, a giant region already active 7 Myr ago and possibly up to 20 Myr ago. Here we analyse Hodge 301 ($\alpha_{2000} = 05^h38^m16^s, \delta_{2000} = -69°03'58''$), one of the oldest structures in 30 Doradus, approximately located at 3 arc-minutes ($\sim$ 44 pc, assuming a distance of 50 kpc) to the northwest of R 136 (Hodge 1988).

Hodge 301 (hereinafter H301) was previously studied by Mendoza V. & Gómez (1973), McGregor & Hyland (1981), Melnick (1985), Lortet & Testor (1991), Walborn & Blades (1997) (hereinafter WB97) and Grebel & Chu (2000) (hereinafter GC00), among others. As a part of an extensive optical spectral classification effort of the stellar populations within the 30 Doradus Nebula, WB97 classified H301 as a cluster in the h and χ Persei phase (namely containing A- and M-type supergiants), with an age $\sim$ 10 Myr, the oldest in the 30 Doradus complex. GC00 used a synergy between spectroscopy, Ultraviolet Imaging Telescope (UIT) photometry and deep WFPC2/HST photometry reaching V$\approx$ 24 to study age, initial mass function (IMF), and reddening of H301. By comparing the loci of main-sequence turn-off (MSTO) and post-MS stars with Padova and Geneva stellar models, they derived an age of 20-25 Myr. Concerning the IMF, for the mass range $1.26-10\,M_{\odot}$ they derived a slope close to Salpeter. Finally, using the UIT photometry they found a mean reddening $E(B-V)=0.28 \pm 0.05$.

More recently, using spectroscopy and a qualitative comparison with the evolutionary models of Brott et al. (2011), Evans et al. (2015) found an age of 15$\pm$5 Myr.

In this paper we rederive H301's age using the photometric capabilities of the survey HTTP[16] (Sabbi et al. 2012, 2015). Figure 1 shows a F555W-band inverted

michele.cignoni@unipi.it
[1] Based on observations with the NASA/ESA Hubble Space Telescope, obtained at the Space Telescope Science Institute, which is operated by AURA Inc., under NASA contract NAS 5-26555
[2] Department of Physics - University of Pisa, Largo Pontecorvo, 3 Pisa, 56127, Italy
[3] Space Telescope Science Institute, 3700 San Martin Drive, Baltimore, MD, 21218, USA
[4] INFN, Largo B. Pontecorvo 3, 56127 Pisa, Italy
[5] European Space Astronomy Centre, Apdo. de Correo 78, E-28691 Villanueva de la Canada, Madrid, Spain
[6] INAF-Osservatorio Astronomico di Bologna, Via Ranzani 1, I-40127 Bologna, Italy
[7] Astronomisches Rechen-Institut, Zentrum für Astronomie der Universität Heidelberg, Mönchhofstr. 12-14, 69120 Heidelberg, Germany
[8] Department of Astronomy, University of Wisconsin-Madison, WI 53706, USA
[9] European Space Research and Technology Centre, Keplerlaan 1, NL-2200 AG Noordwijk, the Netherlands
[10] Zentrum für Astronomie der Universität Heidelberg, Institut für Theoretische Astrophysik, Albert-Ueberle-Str. 2, 69120 Heidelberg, Germany
[11] Max Planck Institute for Astronomy, Konigstuhl 17, D-69117 Heidelberg, Germany
[12] Department of Astrophysics, Radboud University, PO Box 9010, NL-6500 GL Nijmegen, the Netherlands
[13] INAF-NA, Osservatorio Astronomico di Capodimonte, Salita Moiariello 16, I-80131 Naples, Italy
[14] Supernova Ltd, OYV 131, Northsound Rd., Virgin Gorda VG1150, Virgin Islands, UK
[15] European Space Agency and Space Telescope Science Institute, 3700 San Martin Drive, Baltimore, MD 21218, USA

[16] The HTTP Photometric Catalog can be downloaded at https://archive.stsci.edu/prepds/30dor/Preview/observations.html.

grey-scale image of the cluster. The depth of our CMDs (V$\approx$ 26) allows us for the first time in this cluster to reach the magnitude of the PMS turn-on (TOn; V$\approx 24-25$), the point of the color-magnitude diagram (CMD) where the PMS stars join the MS. This stellar feature is used to measure the cluster age in a way that is independent of the previous analysis, mostly based on the MSTO and post-MS stars. For this task we used the synthetic CMD approach which allows us to fit several crucial features of the CMD (MSTO, PMS TOn and field contamination) simultaneously. The advantage with respect to the classical isochrone fitting is the full consideration of evolutionary times, magnitude and color spreads from photometric errors, incompleteness, and unresolved binaries.

The structure of the present paper is as follows. In Section 2 we present the data and we discuss the relevant stellar phases of H301's CMD. In Section 3 we construct a library of synthetic CMDs based on stellar isochrones and we use them to locate the MSTO and TOn in the data. In Section 4 we recover the most likely history for H301. Conclusions close the paper.

2. DATA

The survey HTTP has gathered unprecedented photometric data with the Hubble Space Telescope (HST) over the entire Tarantula Nebula in the near UV (WFC3/UVIS F275W and F336W), optical (ACS/WFC F555W and F658N), and near IR (WFC3/IR F110W and F160W). Here we focus on the optical CMD of H301, the only one deep enough to reach 30 Myr old PMS stars.

Figure 2 shows the density map of the 10 pc region around H301. The cluster centroid was chosen as the point minimizing the distance to all stars.

In order to determine the cluster members, we found the radius at which the stellar density drops to a value indistinguishable from the field. Stars within this radius are assumed to belong to the cluster, and those outside are treated as belonging to the field population.

Figure 3 shows the radial profile (number of stars per pc^2) of H301 as calculated in the quadrants of Fig. 2 (the top-left, top-right, bottom-right, and bottom-left profiles are indicated with green, blue, red, and black slopes, respectively). Despite the slight asymmetry (the top-left profile shows an excess of stars between 1 and 2 pc from the cluster center), we found that a 4 pc radius encloses about 85% of the stars of H301, minimizing at the same time field contamination. Figure 4 shows the corresponding CMD. Photometric errors, as derived from artificial stars tests (see further down in this Section), are also shown on the right side. Important features of this CMD are:

- An extended MS ranging from F555W$\approx$16 to F555W$\approx$26. For stars in the magnitude range 16 <F555W< 18, the MS is broader than expected on the basis of photometric errors (see figure). As already discovered by GC00 (see their Fig. 6), the MS is likely broadened toward the red by the presence of Be stars. Concerning these objects, GC00 also showed that they are most common among the early B-type stars and show the largest Balmer and IR excess for the early types (see also Grebel 1997). In our photometry, 17 stars above F555W$\sim$ 19 show an Hα excess[17] (filled red circles in the figure), as expected in Be-stars. Despite this spread, the clear drop of star counts brighter than F555W$\sim$16 suggests that the MSTO (green dashed line) is not brighter than this magnitude;

- A group of stars up to three magnitudes brighter than the MSTO; the two brightest and the three reddest are presumably He-burning stars of intermediate mass on the blue (blue super giant, BSG) and red (red super giant, RSG) side of the blue loop (BL), respectively. Their membership is certain, as indicated by the plots in Fig. 5, where the CMDs of stars in three different annuli (panels from left to right show stars between 0 and 4 pc, 6.93 and 8 pc, 8 and 8.95 pc from the cluster center) of equal area around the center of H301 are compared. The two outer annuli represent pure field samples and only a few upper-MS stars populate their CMDs above F555W$\sim$ 20. In addition, no upper-MS star above F555W$\sim$ 17 is detected. On the other hand below F555W$\sim$ 22 field contamination increases significantly.

- A group of stars at the right of the MS (indicated with "FC", field contamination, in Figure 4). As suggested by the CMDs of the two outer fields in Figure 5, the entirety of these stars is compatible with being red giant (RGB) and red clump (RC) stars from the field of the LMC. The elongated shape of the field RC (visible in the CMD as the over-density around F555W$\approx$ 20 and color around 1.2$-$1.4) suggests the presence of some differential reddening.

The presence of two blue stars above the MSTO around V$\sim$14-15 magnitudes reflects the well-known problem that while theoretical CMDs predict a post main sequence gap (PMSG) between the end of the main sequence and the presumed core He burning A-supergiants (the two stars near V$\sim$13 magnitudes), this gap is not observed. In clusters of this approximate age the PMSG is populated by bright B-type giants and supergiants (of similar color to the main sequence dwarfs and subgiants), in the case of Hodge 301 these two stars are confirmed cluster members with spectral types B3 Ib and B2 II-III(n)e (see Evans et al. 2015). While the fact that the precursor of SN1987A was a B3 I star (Walborn et al. 1989) indicates that core He burning stars can inhabit this part of the CMD/Hertzsprung Russel diagram (HRD) there is as yet no unambiguous method for distinguishing between core H and He burning blue stars (see Hunter et al. 2008, Vink et al. 2010, Grebel et al. 1996, and McEvoy et al. 2015 for discussions of how rotational velocity distributions, mass-loss considerations and binary frequency might define the width of the main sequence for B-stars in the LMC). For now we will assume that the MSTO is as shown in Fig. 4 but will return to this point in the discussion.

In the next Sections we study the CMD of H301 using the synthetic CMD technique (see, e.g., Cignoni et al.

[17] Measured with respect to the median color F555W-F658W in the F555W-F658W vs F555W-F775W diagram (see De Marchi et al. 2010 for details on this approach).

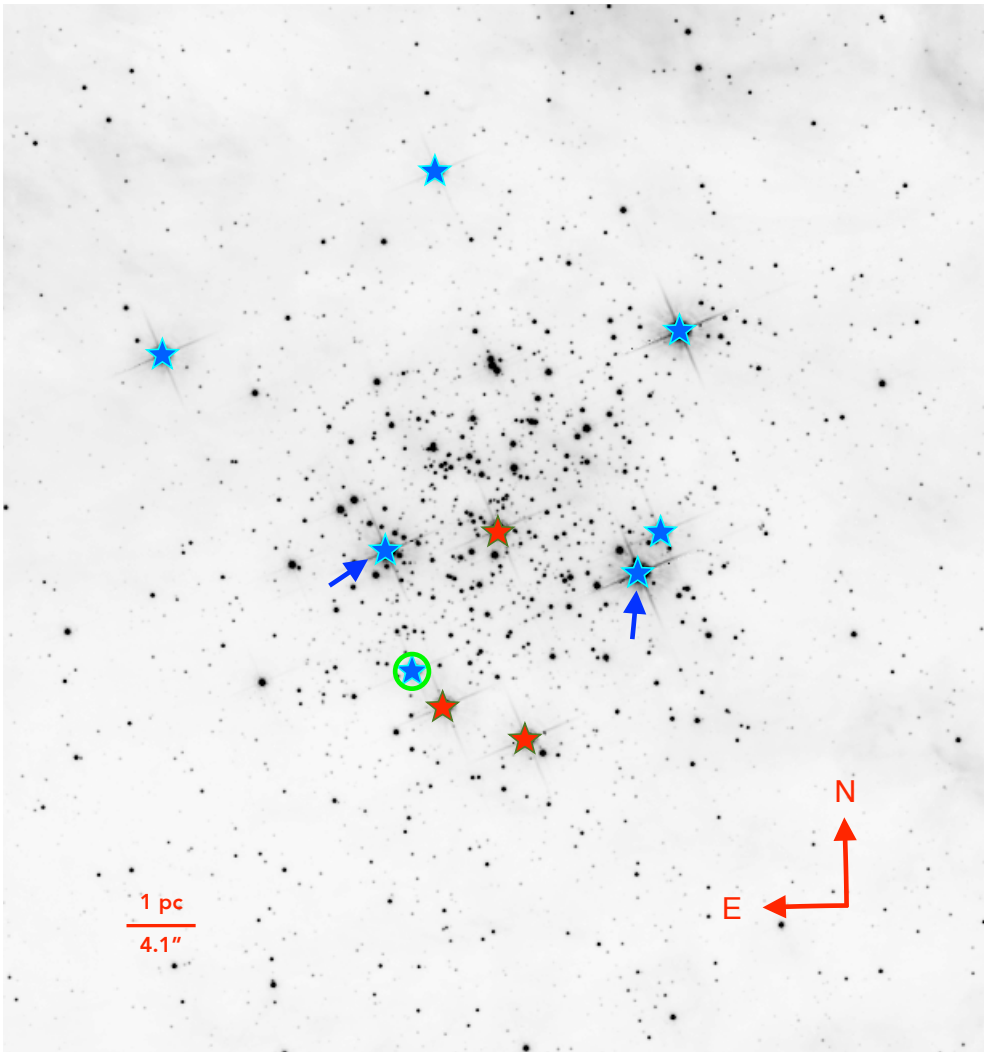

Figure 1. Inverted grey-scale image (F555W) of Hodge 301. Blue (F555W-F775W< 1) and red (F555W-F775W> 1) supergiant stars (F555W< 15) are indicated with blue and red filled starred symbols, respectively. The blue arrows point to the two BSGs discussed in the present analysis (see text). The open green circle indicates a spectroscopic binary (Walborn & Blades 1997) that may have a compact companion.

2015). A mandatory ingredient of this approach is to accurately test photometric errors and incompleteness of the data. Here these tests are conducted following a two step procedure: 1) "fake" sources are injected (one at a time) following a uniform distribution onto the actual images. The source detection routine used for our science images is applied to the fields containing the combined actual images and the fake sources. Counting how many fake stars are lost as a function of magnitude and position provides the map of the local incompleteness. Note that if the latter is averaged over the entire cluster, the result does not represent the "true" average incompleteness, because the distribution of real stars is not uniform; 2) the local incompleteness is used to restore the real profile of the cluster (before the incompleteness). Fake stars are now injected (one at a time) onto the actual images following this profile and the source detection routine is applied again. Although the resulting incompleteness is locally identical to the incompleteness of step 1, its average over the entire cluster is an unbiased estimate

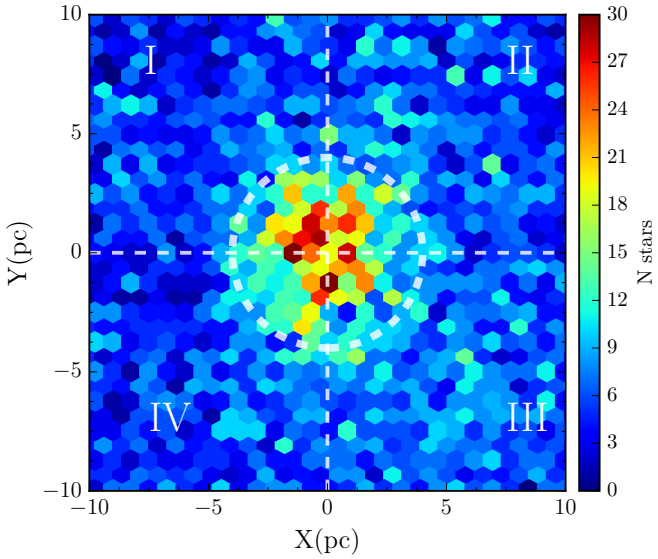

Figure 2. Spatial distribution of H301. 1 pc corresponds to ≈ 4 arcseconds. The central hole is an artifact of the incompleteness, due to the severe central crowding. The dashed circle indicates a 4 pc radius.

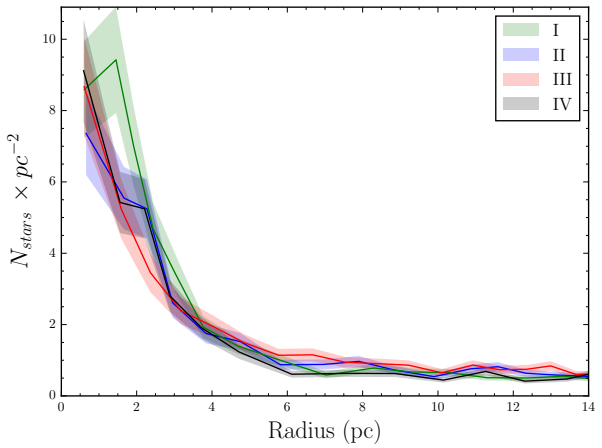

Figure 3. Radial profiles of H301 in four quadrants (see Fig. 2). The shadowed areas show the Poissonian uncertainties. The differences in one quadrant (green) may indicate that the cluster is not spherical.

of the "true" average incompleteness. Figure 6 shows the average completeness level for the filters F555W and F775W.

3. SYNTHETIC CMDS

Synthetic CMDs are generated using the latest PARSEC (Bressan et al. 2012; Tang et al. 2014) isochrones, and assuming a Kroupa IMF and metallicity Z=0.008 (from the mean [Fe/H] for LMC Cepheids of Luck et al. 1998, referred to the updated Caffau et al. 2011 mixture). 30% of synthetic stars are considered members of binary systems and their flux is combined with a secondary star sampled from the same IMF. To mimic the observational process, each synthetic CMD is then convolved with photometric errors (derived from the cumulative distribution of mag_{out}-mag_{input} of fake stars) and incompleteness as derived in the previous Section.

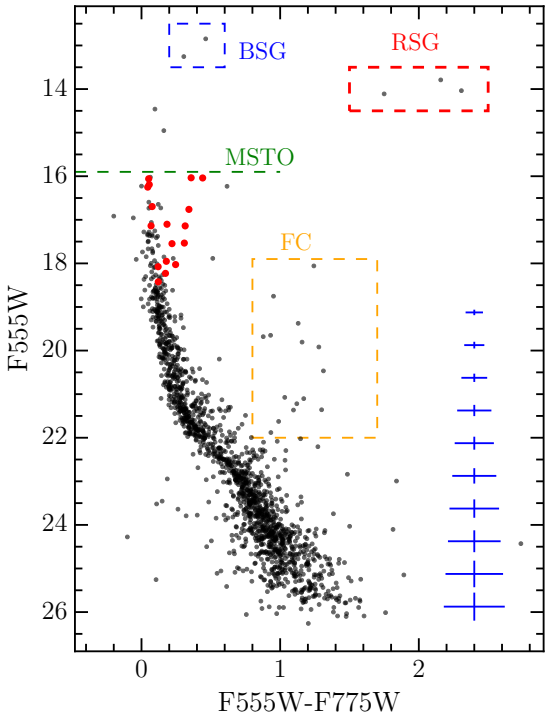

Figure 4. F555W vs F555W-F775W CMD of H301 within 4 pc from the cluster center. Relevant stellar species and contamination are highlighted. Red circles indicate stars brighter than F555W∼ 19 characterized by Hα excess.

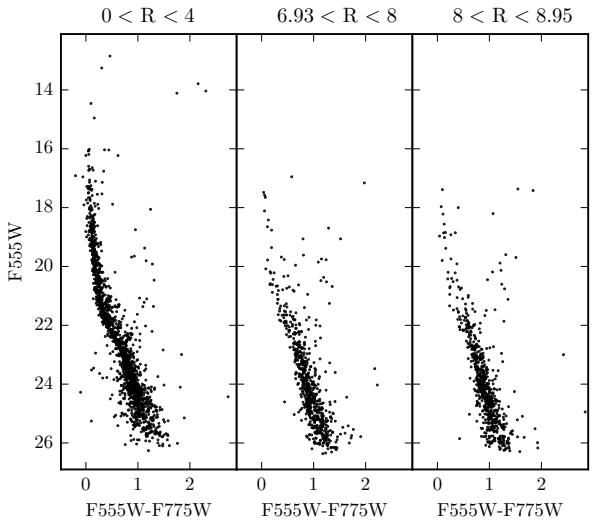

Figure 5. From left to right, CMD of stars between 0 and 4 pc, 6.93 and 8 pc, 8 and 8.95 pc from the center of H301.

We have compared our synthetic CMDs with the massive stars and low-mass ones of H301.

Massive stars: Given the likely range of ages of H301, 10-30 Myr, MSTO and BL phases are populated by stars more massive than 7 $M_\odot$. Figure 7 shows four synthetic

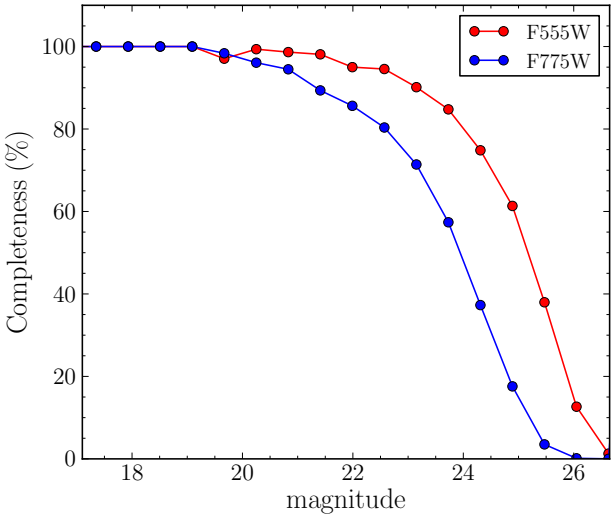

Figure 6. Average photometric completeness in F555W (red symbols) and F775W (blue symbols).

populations of the labeled ages (15, 20, 25 and 30 Myr) and a duration of star formation of 1 Myr overlaid to the observations. In order to increase the visibility of the models in the fastest evolutionary phases, the synthetic CMDs are populated with a number of stars much larger the observed counterpart.

The distance modulus is assumed equal to 18.5 (see e.g. Panagia et al. 1991; Pietrzyński et al. 2013) and the total reddening, E(B−V)≈ 0.22, is chosen by fitting the average color of the UMS in the magnitude range 18−20. Note that through this paper the total reddening is defined as the composition of the Milky Way foreground reddening, kept fixed at E(B−V)≈ 0.07 with $R_V = 3.1$, and the local reddening. For the latter we used the A_λ values from De Marchi et al. (2016), which are specifically derived for the 30 Doradus environment. An inspection of Figure 7 reveals that: 1) only ages in the range 15-25 Myr allow one to match color and magnitude of the BL. The synthetic BL of the 15 Myr isochrone fits the magnitude of the two BSGs (although it is too blue), but it is clearly too bright on the red side. On the other hand, the 20 Myr isochrone fits well the magnitude of the three RSGs, but it fails to reproduce the ratio RSGs/BSGs (the BL color extension is too short and its morphology resembles a red clump); 2) Concerning the MSTO, even considering photometric errors, none of the models is able to reproduce the observed color spread in the magnitude range 16 − 18. This is not surprising given the presence of Be stars, which are thought to be fast rotators surrounded by an out-flowing equatorial disk, likely causing their infrared excess (see e.g. Porter & Rivinius 2003); 3) only isochrones between 25 Myr and 30 Myr allow one to reproduce the MSTO luminosity (V∼ 16; corresponding to a mass ≈ 9 $M_\odot$ with PARSEC models), while the younger ones are at least 1 mag brighter than the MSTO tip .

Low mass stars: The PMS TOn is the point where the PMS joins the MS. In H301 this phase is populated by low-mass stars below 1.5 $M_\odot$. According to stellar evolution theory, at the magnitude of the TOn, the luminosity function (LF) of a simple population is characterized

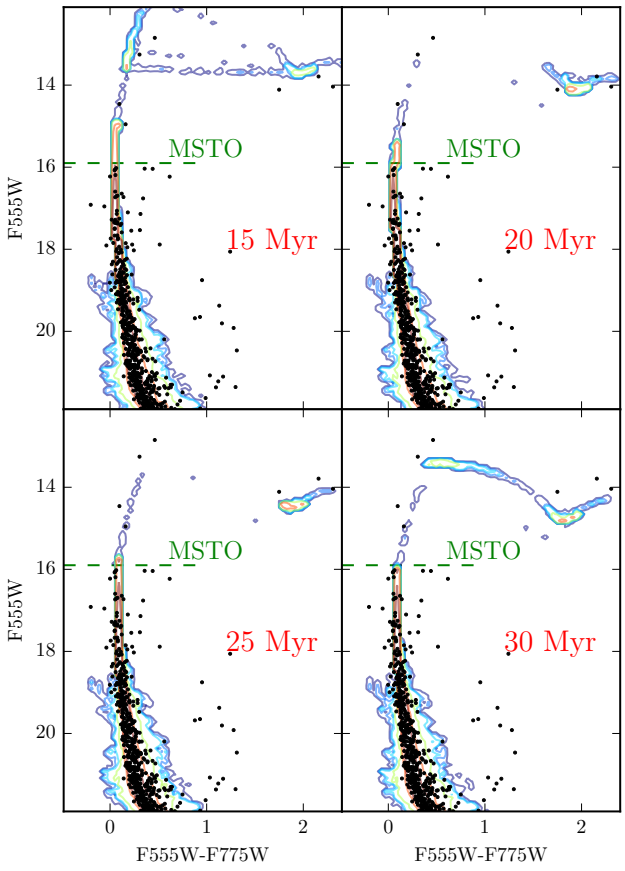

Figure 7. Synthetic CMDs (colored contours) for populations of the labeled ages, taking unresolved binaries and photometric errors into account, overlaid on the F555W vs F555W−F775W CMD (dots) of H301.

by a strong peak followed by a dip (see, e.g., Cignoni et al. 2010). This behavior is clearly visible in the top panel of Fig. 8 where synthetic populations of different ages are shown (note that only photometric errors are applied, while the incompleteness is not). The older the age of the cluster, the fainter the LF TOn peak and the corresponding dip. Peak and dip respectively reflect the steep dependence of stellar mass on magnitude near the TOn and the following flattening below the TOn, caused by the short evolutionary timescale of the PMS phase compared to the MS. After the dip, the shape of the LF mimics the IMF, rising with decreasing stellar mass. For comparison, the dashed line shows a synthetic zero age MS where the PMS phase has been artificially suppressed: as expected, without PMS there is no TOn peak/dip and LF increases monotonically.

From a theoretical point of view, the dependence of TOn luminosity on the PMS evolutionary times is a serious issue. However, while in the first few Myr, PMS times are affected by several uncertainties like, e.g., the initial conditions (in particular the initial radius), the efficiency of convection, the initial abundance of deuterium and the accretion rate (see, e.g., Baraffe et al. 2002, Tognelli et al. 2011), at later times PMS tracks

tend to converge. Indeed, the zero age MS position for 1 $M_\odot$ does not show significant differences among different authors (see Fig. 14 in Tognelli et al. 2011), with a dispersion in $\log(L/L_\odot)$ of ≈ 0.1 dex. In terms of age, such an uncertainty corresponds to an age error smaller than 3 Myr at 30 Myr.

Concerning the observational errors, two things limit the TOn visibility in H301: incompleteness and field contamination. For ages older than 15 Myr, at the distance of the LMC, a TOn is fainter than 23 in V magnitude, ~ 24.5 at 30 Myr. At these levels of faintness, incompleteness can be severe, especially in the center of H301. At odds with the massive stars, where the degree of contamination is negligible, at faint magnitudes it can bias the age, mimicking an older population.

The bottom panel of Figure 8 shows the observed LFs, corrected for the incompleteness, of stars in five concentric annuli of equal area around the center of H301 (in red, blue, magenta, green and black stars between 0 and 2.91 pc, 2.91 and 4.11 pc, 4.11 and 5.04 pc, 5.04 and 5.82 pc, 5.82 and 6.51 pc, respectively). The hatched area fainter than V=25.25 indicates where the incompleteness in the innermost annulus drops below 50%.

The TOn feature is visible as the narrow peak near V $\sim$ 24.25 in the LF of the innermost region (red histogram). At fainter magnitudes the LF increases following the IMF, then it drops again at V> 25.25. This is because below this limit the LF becomes increasingly affected by photometric blends, whose net effect is to brighten the sample and deplete the faint end. This happens for all annuli, but increases at progressively fainter magnitudes as the distance from the cluster center decreases. Indeed, the blue and magenta LFs (second and third innermost annuli, respectively) show a general increase up to V=26, reflecting the much more favorable incompleteness (below 50% only at V> 26). However, the higher field contamination reduces the TOn visibility, which is only noticeable as a broad peak in the magnitude range $24 - 24.75$

Finally, the green and black LFs (the outermost annuli) show a smooth increase, with no bumps in the range 24−25, as expected for the average field of the LMC.

From a comparison by eye with the synthetic LFs we estimate the TOn age to be between 26 and 30 Myr.

In the next Section we derive the most likely SFH compatible with the data.

4. QUANTITATIVE DERIVATION OF H301'S SFH

To recover the most likely SFH we used the hybrid-genetic code SFERA (Star Formation Evolution Recovery Algorithm), the statistical approach described by Cignoni et al. (2015). Metallicity, binary fraction and distance modulus are initially kept fixed at Z= 0.008, 30% and 18.5, respectively, while age, reddening and field contamination are free parameters. The SFH is parameterized in 40 contiguous steps of duration 1 Myr between now and 40 Myr ago. The best combination of synthetic CMDs and field contamination (a template field is taken at radii larger than 6 pc from the center) is searched by SFERA. In SFERA, observational and model CMDs are binned in color and magnitude, and the binning scheme is changed randomly. The two 2D distributions are then compared with a Poissonian χ^2.

In order to reduce as much as possible the field contamination we only used stars within 4 pc from H301's center. As a first step, we recovered the SFH using massive stars (MSTO) and low-mass stars (TOn stars) independently. The former includes all stars brighter than F555W= 19, the latter all stars fainter than F555W= 22. Figure 9 shows the results, with the MSTO/BL solution (given the paucity of BL stars, the age is largely driven by the MSTO) in dashed green and PMS TOn one in solid blue. Finally, the red solid line shows the SFH inferred using the entire CMD. In all cases the most relevant peak is located in the range 28.5-31.5 Myr. The MSTO/BL solution shows a clear peak at 30.5^{+1}_{-2} Myr, while the TOn peak is slightly broader on the young side, suggesting that the MSTO age is better defined (not surprising given the much smaller photometric error affecting this phase). The net result is that, within the errors, MSTO and TOn ages are in excellent agreement. Combining the two features leads to the red solid line solution, which resembles more the MSTO solution, but with smaller uncertainties. Hereafter we refer to this solution as the best SFH for H301.

At first glance our conclusions seem at odds with the results derived by Naylor (2009), who studied the age for a selection of clusters and associations younger than 100 Myr. They found that the ages based on PMS isochrones are 1.5-2.0 times shorter than the "nuclear" MSTO ages. However, our PMS age is mostly based on the TOn luminosity, and not on the PMS stars, whose color is affected by several uncertainties (see e.g. Hennekemper et al. 2008). Another possible source of error is the use of different sets of models to study different phases: we do not have this kind of problem because in this work we used the PARSEC models which follow the entire evolution from the PMS to the post-MS.

Fig. 10 shows the synthetic LF (blue line) corresponding to the best SFH compared with the observed counterpart (red line). Error bars in the data are the square root of the counts, while the $1\,\sigma$ uncertainty in the model is indicated with a blue band. The quality of the fit is excellent and most of the differences are within the errors. We found a best-fitting E(B−V) of 0.22-0.24 mag with a $1\,\sigma$ dispersion of 0.04 mag. In this case the dispersion is not the actual error, but the spread (differential reddening) needed to match the MS width.

It is worth to notice that the inferred absolute ages are expected to change according to the adopted distance modulus. Indeed a shorter distance would increase the cluster age. However, in the range 20-30 Myr, both the MSTO and TOn magnitudes change with age by ≈ 0.1 mag/Myr, hence the relative age MSTO/TOn remains unchanged.

In order to derive the initial total mass and number of supernovae Type II exploded in H301 we ran 1000 Monte Carlo simulations normalized to the observed number of stars (decontaminated with an external field) brighter than F555W = 20. Adopting the peak age 30.5 Myr, we calculated that the initial total mass of H301 was $\approx 8800 \pm 800$ $M_\odot$[18] and that 52 ± 9 supernovae Type II[19] exploded. This result is also supported by obser-

[18] Corrected for stars residing outside the 4 pc radius (about 15%).

[19] Assuming that all stars above about 20 $M_\odot$ produce black holes.

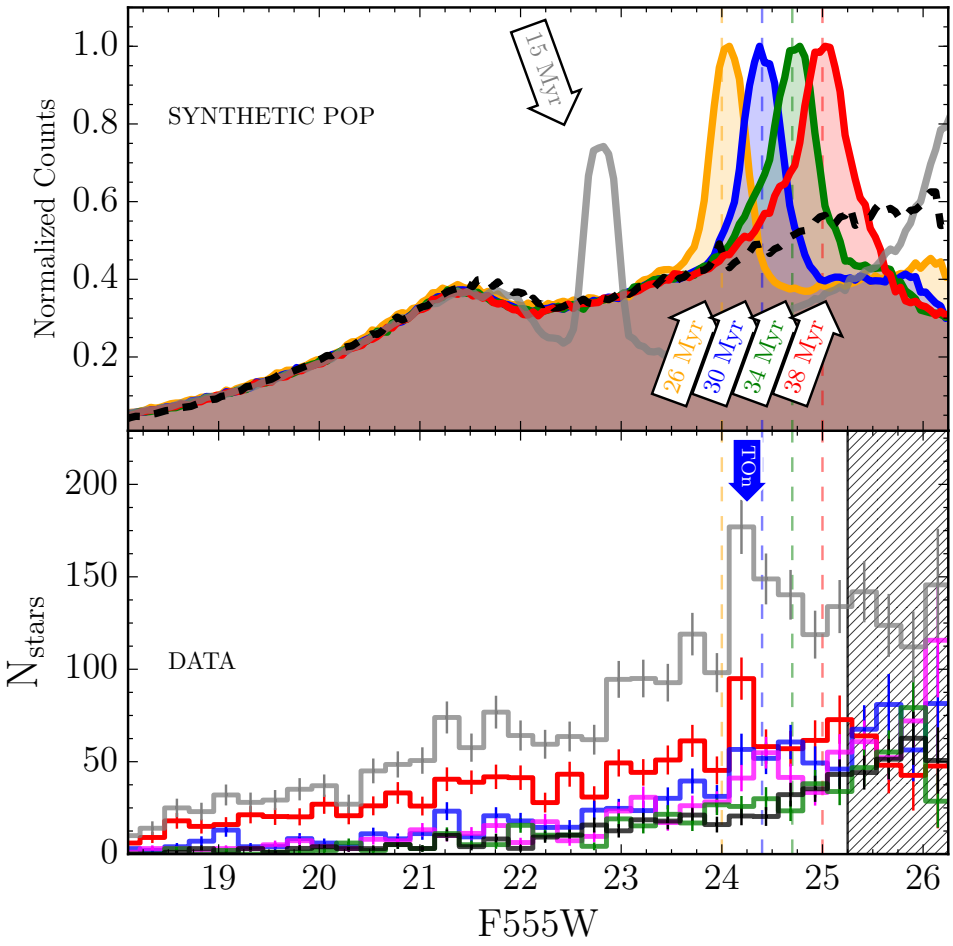

Figure 8. Top panel: synthetic LFs for the labeled ages. The thick dashed line shows a synthetic zero age MS where the PMS phase has been artificially suppressed. Bottom panel: Observed LFs of stars in equal area annuli around H301's center (red for stars within 2.91 pc, blue between 2.91 and 4.11 pc, magenta between 4.11 and 5.04 pc, green between 5.04 and 5.82 pc, black between 5.82 and 6.51 pc). The grey histogram is the sum of the three innermost LFs. The magnitude of the TOn is also indicated.

vations (see GC00 and references therein; Lopez et al. 2011), that place H301 within an high-velocity expanding shell, caracterized by multiple centers and filled with diffuse X-ray emission. Moreover, Walborn & Blades (1997) classified an object, WB9 (Be1 in GC00; indicated with a green circle in Fig. 1), as a spectroscopic binary with a compact companion, possibly the stellar remnant of a supernova event.

Before closing this section, it is important to discuss the impact of the assumed binary recipe and metallicity on the recovered SFH.

4.1. *Binaries*

Although our findings do not critically depend on the adopted binary fraction and mass ratio, a very high binary fraction (above 50%; Sana et al. 2013) and flatter mass ratio q (our binary prescription favors low q binaries), as found for O-stars, can affect the recovered SFH. In practice, the effect of equal mass binaries is to make stars appear 0.75 mag brighter, and not taking it into account leads to an underestimate of the age. Since our SFHs are derived disfavouring q=1 massive binaries we may indeed interpret the observed brightnesses underestimating the age if the binaries have mostly the same mass.

However, B-type stars may behave differently. Dunstall et al. (2015) studied the multiplicity of 408 B-type stars observed in different regions (NGC 2070, NGC 2060, Hodge 301, SL 639) of 30 Doradus with multi-epoch spectroscopy from the VLT-FLAMES Tarantula Survey (VFTS). Although they found an average binary fraction of about 58%, close to the O-stars multiplicity by Sana et al. (2013), the intrinsic binary fraction in H301 was found to be remarkably low and around 20% (8% detected, with a detection probability of $40 \pm 10\%$). Concerning the mass ratio, they found a distribution of q favoring low-mass companions ($f(q) \propto q^{-2.8}$).

Although our binary prescription is consistent with Dunstall et al.'s 2015 finding, we also tested the hypothesis of a binary population similar to that found by Sana et al. (2013) for O-type stars. Figure 11 shows the SFH recovered assuming a binary fraction of 50% and a uniform distribution of q. Overall, the result is qualitatively similar to the standard SFH, except the peak that is slightly

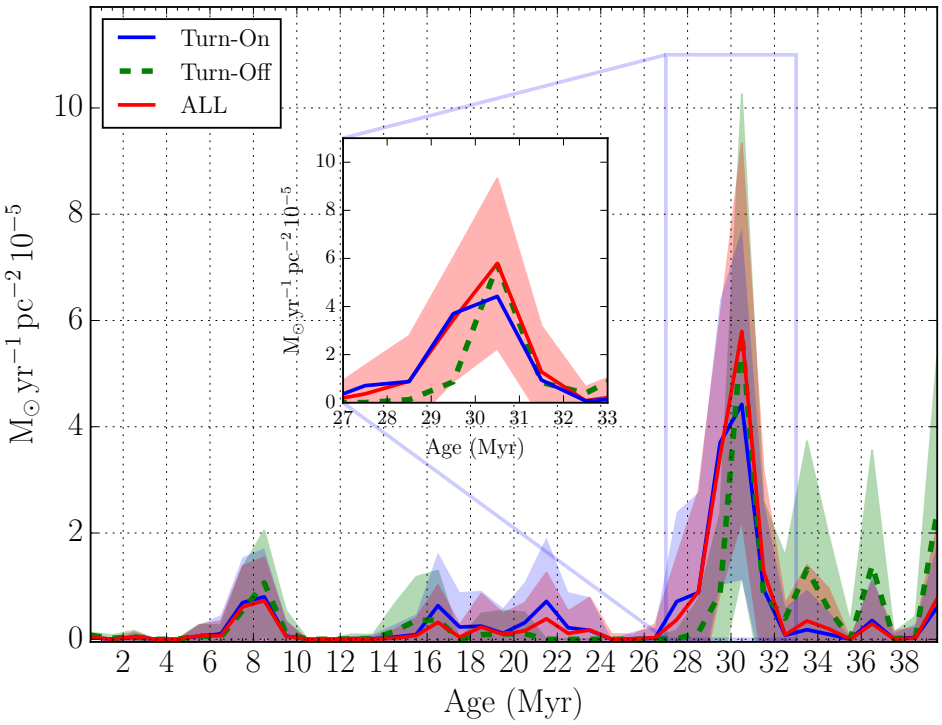

Figure 9. SFHs of H301. Solid red, blue and dashed green lines corresponds to the best SFHs obtained using the entire CMD, TOn alone and MSTO/BL alone, respectively. Shaded regions represent the 1 σ standard deviation from the best SFH. The inset panel zooms around the main peak.

broader.

Finally, in the literature there is no evidence of a universal mass ratio holding from massive to low-mass stars (seey e.g. Ward-Duong et al. 2015). However, the similarity of our inferred MSTO and TOn ages suggests that binary populations of high and low-mass stars are not dramatically different.

4.2. *Metallicity*

The empirical evidence of a metallicity spread in the young populations of the LMC (see e.g. Luck et al. 1998, Romaniello et al. 2008) makes Hodge's metallicity inherently uncertain. In order to test the impact of a lower metallicity on the final age, we re-recovered the SFH using PARSEC models with Z=0.005 (about 1 σ away from the mean value of Luck's sample). The result is shown in Fig. 12. The lower metallicity reduces the peak age by about 3 Myr. In this case, the best age is 27.5 ± 1 Myr.

This difference can be explained by the dependence of MSTO and TOn luminosities on metallicity and helium abundance (PARSEC isochrones at Z=0.005 have slightly lower helium abundance than isochrones at Z=0.008). First, the lower the metallicity, the shorter the evolutionary timescale of a star of a given mass during the major evolutionary phases. For this reason, at a fixed age, MSTO and TOn masses are lower at Z=0.005 than at Z=0.008, and stars of lower masses are also fainter. However, as secondary effect, a decrease of metallicity shifts the isochrone to higher luminosities, whereas a decrease of helium has the opposite effect. The combined effect of these changes decreases MSTO and TOn luminosities of 0.1-0.2 mag, mimicking an older isochrone. The resulting mean reddening is also higher by about 0.02 mag (E(B-V)=0.24 mag), which causes a further luminosity decrease of about 0.1 mag.

The new peak age, 27.5 Myr, leaves the initial total mass of H301 almost unchanged, whereas the number of supernovae Type II, 46 ± 8, is slightly lower than in the Z=0.008 case.

Another effect of the lower metallicity is to increase the luminosity of the BL phase. This is clearly visible in Fig. 13. In contrast to Z=0.008 isochrones (see Fig. 7), the 20 Myr BL is long enough to reach the color of the two BSGs, but the red side is now brighter than the three RSGs. On the other hand, the 25 Myr isochrone plays the same role of the 20 Myr isochrone at Z=0.008, fitting well the RSGs luminosity but failing to reproduce the observed ratio RSGs/BSGs. The entire 30 Myr BL is too faint. In conclusion, while no one model is able to reproduce extension and luminosity of the BL at the same time, the 25 Myr is the one that better represents the observed BL, getting closer to the MSTO/TOn best ages, which are now only 2.5 Myr apart.

In summary, given the uncertainty in the metallicity of H301, we conclude that the best fitting age is between 26.5 and 31.5 Myr, while the predicted number of supernovae Type II is between 38 and 61.

5. COMPARISON WITH THE LITERATURE

Compared to the literature, our lower limit on the age of H301, $\sim$ 26.5 Myr, is slightly older than the photometric estimate of GC00, who found 20 ± 5 and 25 ± 5 Myr using Geneva (Schaerer et al. 1993) and Padova models (Bertelli et al. 1994) respectively. GC00 required their

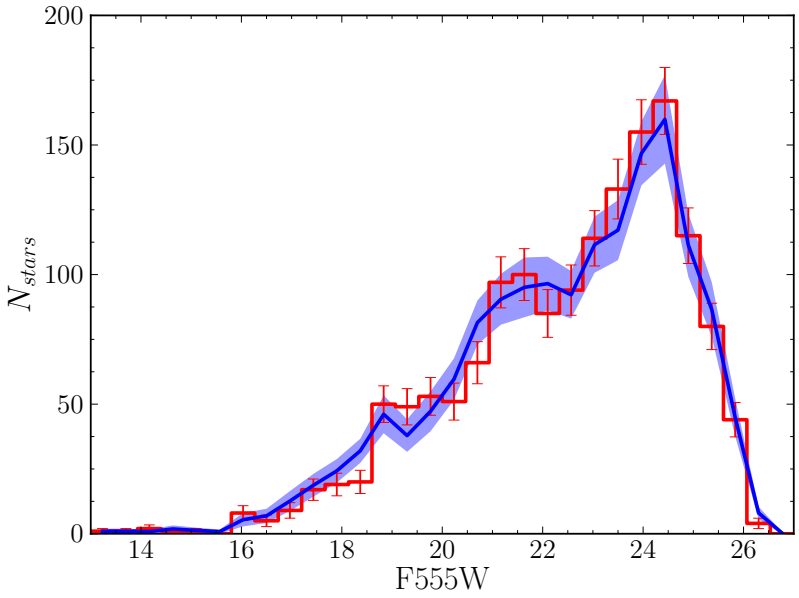

Figure 10. Synthetic LF generated with the most likely SFH compared with the observational LF.

isochrone fit to match the position of the blue and red supergiants and omitted stars with Hα excess. This difference is probably caused by the different versions of the isochrones and different stellar phases used in our analysis. Indeed, if we limit our analysis to the BL phase only (see Fig. 7 and 13), our best estimate of the age would drop down to 20-25 Myr, in good agreement with GC00. GC00's estimate of the total reddening (E(B-V)$= 0.28 \pm 0.05$ mag) is compatible with our estimate.

Concerning the mass of H301, GC00 found a present day mass of 4882$\pm$247 M$_\odot$ between 0.4 and 12 M$_\odot$, corresponding to an initial mass of $\approx 6000 \pm 525$ M$_\odot$ when extrapolated with a Salpeter IMF above 12 and up to 120 M$_\odot$. Most of the difference from our estimate stems from the different age and IMF. If we were to adopt a Salpeter IMF in our models down to 0.4 M$_\odot$, our mass estimate would drop to $\sim 7200 \pm 700$ M$_\odot$. In addition, if we were to adopt a 20 Myr isochrone (as adopted by GC00) instead of a 30.5 Myr ago, our result would drop to 6600 ± 400 M$_\odot$, in excellent agreement with GC00's estimate. Our estimated number of supernovae, between 38 and 61, is in good agreement with GC00's rate (41$\pm$7).

Our best age is higher than that found by Evans (15$\pm$5 Myr), who used high resolution spectroscopy to reconstruct temperature and luminosity for a sample of B-stars within 4.9 pc from H301's center. Part of the discrepancy can be ascribed to the adopted stellar models from Brott et al. (2011), whose timing is faster than our Padova models of the same metallicity: we found that a Padova isochrone of 30 Myr has the same MSTO luminosity of Brott et al. isochrone of 25 Myr. The rest of the discrepancy might then be attributed to two other potential effects; the choice MSTO magnitude in the present paper (Fig. 4 and see the accompanying discussion in section 2), and the transformation from a CMD to the HRD in Evans et al. It is clear from Fig. 5 of Evans et al. that they include the fainter of the two PMSG stars in their main sequence group, and from our Fig.6 one might argue that raising the MSTO to V$=$ 15 would give an age of 20 Myr, in better agreement with Evans et al. However a more serious issue perhaps is that Evans et al. derive luminosities from the stars' effective temperatures that imply there are several stars in H301 with masses between 12 and 15 solar masses, significantly in excess of the 9-10 M$_\odot$ implied by an age of 26.5-31.5 Myr of the PARSEC models. The brightest of these B-stars, particularly those in the PMSG, might be explained as blue stragglers, being the products of binary evolution. The present low fraction of binaries in H301, discussed in the previous section, may simply reflect that many of these have already interacted and formed binary products as discussed by Schneider et al. (2014) producing blue straggler stars that are among the brightest blue stars in H301.

Finally, it is important to remark that a 15 Myr age would be strongly ruled out by the PMS TOn. As shown in Fig. 8, a TOn of 15 Myr (grey slope) would be at least 1 mag brighter than the present TOn, and hence less affected by photometric errors and incompleteness. If any significant excess of counts at V$\approx 22.5 - 23$ were present, it would be clearly detected. Moreover, the 15 Myr age is disfavored by the MSTO too: as shown in Fig. 7, the isodensity contours of the 15 Myr model show a continuity of counts up to the two PMSG stars, while no stars are observed in the magnitude range 15-16.

We further note, that a search for PMS stars based on the Hα excess emission (e.g. De Marchi et al. 2010, 2011) over the whole HTTP area has revealed an overdensity of about 120 PMS stars within 4 pc of H301, with an average age of $\sim$ 28 Myr (De Marchi, Panagia, Sabbi, et al., in preparation), hence in excellent agreement with our estimate.

Although of low significance, a mild activity in the range 6-8 Myr is also predicted by most of our solutions. Indeed, for V$>$ 23, a few stars up to 0.5 mag redder than the MS are visible at all radii (see Fig. 5), hence suggesting that if a more recent episode of star formation took place this did not stem necessarily from H301 but

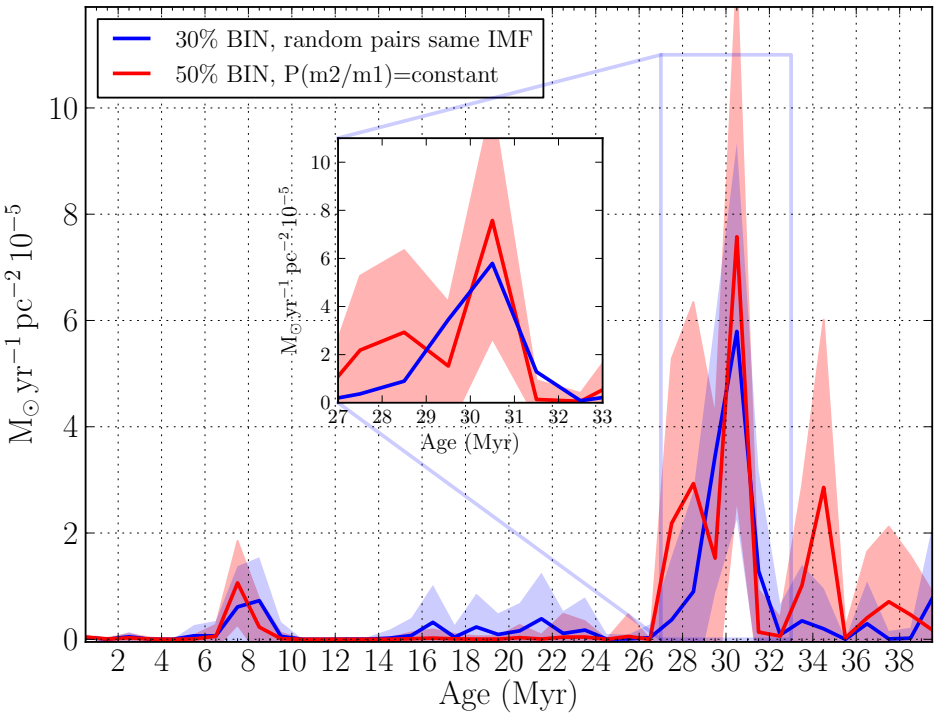

Figure 11. Red slope: SFH recovered adopting 50% of binaries and constant mass ratio.

it involved a larger region, as generated in a more diffuse environment or from a dissolved cluster. An inspection of the Hα flux reveals that some of these red objects have Hα excess, but their signal-to-noise ratio is too low ($1-2\,\sigma$) for a firm conclusion. Another possibility is that a few stars in the region suffer from much higher reddening, mimicking a PMS population.

6. CONCLUSIONS

From comparison of the observed CMD with simulations based on stellar evolutionary models we derive in a self-consistent way the age distribution and reddening of Hodge 301, a young cluster located in the 30 Doradus region. Thanks to the photometric capabilities of the HTTP data-set we have detected the PMS TOn for the first time. The peak age we derive from fitting this feature and the MSTO, between 26.5 and 31.5 Myr (30.5^{+1}_{-2} Myr using Z=0.008, 27.5 ± 1 Myr using Z=0.005), confirms that Hodge 301 is much older than the bulk of the stars in NGC 2070, the most active region of 30 Doradus, but only slightly older than its oldest stars ($\approx$ 20 Myr; Cignoni et al. 2015). For a fixed metallicity, the resulting age spread, $\approx 1-3$ Myr, is of the order of the age uncertainty as expected from photometric errors only, hence it is difficult to conclude whether the spread reflects a real prolonged SF.

The inferred PMS TOn age is consistent with the age derived from the MSTO and a few Myr older than the age derived from fitting the luminosity of the post-MS stars. In particular, while none of the models can reproduce BL extension and luminosity at the same time, fitting the three RSGs leads to an age between 20 and 25 Myr. However, post-MS theoretical models for intermediate/massive stars are very uncertain. As shown in, e.g., Tang et al. 2014 mass loss and core-convective overshooting can greatly affect the BL color extension. Indeed, models tend to predict a clear separation in the CMD between MS and BL stars, while no such gap is seen in several extragalactic young massive star clusters (see e.g. Larsen et al. 2011) and dwarf galaxies (see e.g. Tang et al. 2014, 2016). Given this uncertainty, we are inclined to favor a cluster age that is mainly derived from fitting the MSTO and PMS TOn. More in general, while the absolute age of H301 does depend on the stellar models adopted, the age difference between H301 and NGC2070 (Cignoni et al. 2015) is robust, since the analysis is done with the same technique, stellar models and clock (PMS TOn).

Finally, it is intriguing that the MSTO/PMS TOn age estimate is also older than the spectroscopic age derived by Evans et al. (2015). Part of the discrepancy could be attributed to the presence of blue stragglers. However, unless H301 hosts an unusual number of these objects, the discrepancy could indicate problems in current stellar evolutionary models of massive stars.

Other interesting results are: 1) H301's total stellar mass is $\approx 8800 \pm 800$ $M_\odot$; 2) the total reddening E(B$-$V) is $\approx 0.22-0.24$ mag, with a dispersion of 0.04 mag; 3) between 38 and 61 supernovae Type-II exploded in the region.

From the point of view of the Tarantula Nebula, the old age of H301, several Myr older than the nearby and massive NGC 2070, and its high supernovae activity, along with the fact that not older clusters are visible in the region, could suggest that the onset of H301 sparked the formation of NGC 2070.

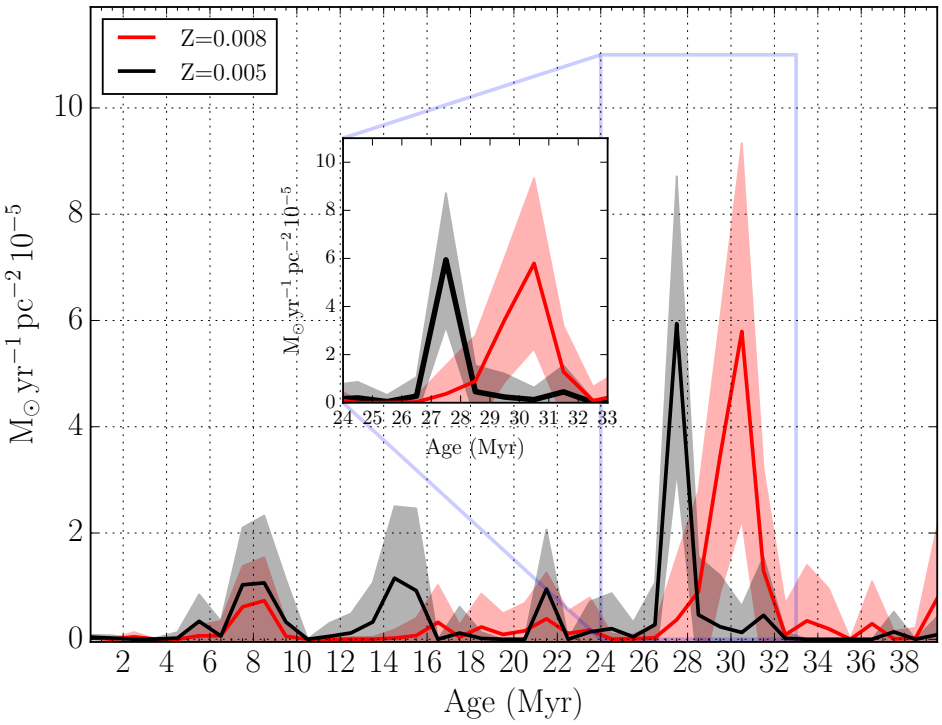

Figure 12. Recovered SFH for the metallicity Z=0.005 (black line) compared to the Z=0.008 one (red line).

We would like to thank Mario Gennaro, Chris Evans and Pier Giorgio Prada Moroni for helpful comments and discussions. D.A.G. kindly acknowledges financial support by the German Research Foundation (DFG) through grant GO 1659/3-2. EKG gratefully acknowledges funding from Sonderforschungsbereich "The Milky Way System" (SFB 881) of the German Research Foundation (DFG), especially via subproject B5.

REFERENCES

Baraffe, I., Chabrier, G., Allard, F., & Hauschildt, P. H. 2002, A&A, 382, 563
Bertelli, G., Bressan, A., Chiosi, C., Fagotto, F., & Nasi, E. 1994, A&AS, 106,
Bressan, A., Marigo, P., Girardi, L., et al. 2012, MNRAS, 427, 127
Brott, I., de Mink, S. E., Cantiello, M., et al. 2011, A&A, 530, A115
Caffau, E., Ludwig, H.-G., Steffen, M., Freytag, B., & Bonifacio, P. 2011, Sol. Phys., 268, 255
Cignoni, M., Tosi, M., Sabbi, E., et al. 2010, ApJ, 712, L63
Cignoni, M., Sabbi, E., van der Marel, R. P., et al. 2015, ApJ, 811, 76
De Marchi, G., Panagia, N., & Romaniello, M. 2010, ApJ, 715, 1
De Marchi, G., Paresce, F., Panagia, N., et al. 2011, ApJ, 739, 27
De Marchi, G., Panagia, N., Sabbi, E., et al. 2016, MNRAS, 455, 4373
Dunstall, P. R., Dufton, P. L., Sana, H., et al. 2015, A&A, 580, A93
Evans, C. J., Kennedy, M. B., Dufton, P. L., et al. 2015, A&A, 574, A13
Grebel, E. K., Roberts, W. J., & Brandner, W. 1996, A&A, 311, 470
Grebel, E. K. 1997, A&A, 317, 448
Grebel, E.K., Chu, Y.-H., 2000, AJ, 111, 787
Hénault-Brunet, V., Evans, C. J., Sana, H., et al. 2012, A&A, 546, AA73
Hennekemper, E., Gouliermis, D. A., Henning, T., Brandner, W., & Dolphin, A. E. 2008, ApJ, 672, 914-929
Hodge, P. 1988, PASP, 100, 1051
Hunter, I., Lennon, D. J., Dufton, P. L., et al. 2008, A&A, 479, 541
Kroupa, P. 2001, MNRAS, 322, 231
Larsen, S. S., de Mink, S. E., Eldridge, J. J., et al. 2011, A&A, 532, A147
Lopez, L. A., Krumholz, M. R., Bolatto, A. D., Prochaska, J. X., & Ramirez-Ruiz, E. 2011, ApJ, 731, 91
Lortet, M.-C., & Testor, G. 1991, A&AS, 89, 185
Luck, R. E., Moffett, T. J., Barnes, T. G., III, & Gieren, W. P. 1998, AJ, 115, 605
McEvoy, C. M., Dufton, P. L., Evans, C. J., et al. 2015, A&A, 575, A70
McGregor, P. J., & Hyland, A. R. 1981, ApJ, 250, 116
Melnick, J. 1985, A&A, 153, 235
Mendoza V., E. E., & Gómez, T. 1973, PASP, 85, 439
Naylor, T. 2009, MNRAS, 399, 432
Panagia, N., Gilmozzi, R., Macchetto, F., Adorf, H.-M., & Kirshner, R. P. 1991, ApJ, 380, L23
Pietrzyński, G., Graczyk, D., Gieren, W., et al. 2013, Nature, 495, 76
Porter, J. M., & Rivinius, T. 2003, PASP, 115, 1153
Romaniello, M., Primas, F., Mottini, M., et al. 2008, A&A, 488, 731
Sabbi, E., Lennon, D. J., Gieles, M., et al. 2012, ApJ, 754, LL37
Sabbi, E., Lennon, D. J., Anderson, J., et al. 2016, ApJS, 222, 11
Sana, H., de Koter, A., de Mink, S. E., et al. 2013, A&A, 550, A107
Schaerer, D., Meynet, G., Maeder, A., & Schaller, G. 1993, A&AS, 98, 523
Schneider, F. R. N., Izzard, R. G., de Mink, S. E., et al. 2014, ApJ, 780, 117
Tang, J., Bressan, A., Rosenfield, P., et al. 2014, MNRAS, 445, 4287
Tang, J., Bressan, A., Rosenfield, P., et al. 2014, MNRAS, 445, 4287
Tang, J., Bressan, A., Slemer, A., et al. 2016, MNRAS, 455, 3393

Tognelli, E., Prada Moroni, P. G., & Degl'Innocenti, S. 2011, A&A, 533, A109
Vink, J. S., Brott, I., Gräfener, G., et al. 2010, A&A, 512, L7
Walborn, N. R., Prevot, M. L., Prevot, L., et al. 1989, A&A, 219, 229
Walborn, N. R., & Blades, J. C. 1997, ApJS, 112, 457
Ward-Duong, K., Patience, J., De Rosa, R. J., et al. 2015, MNRAS, 449, 2618

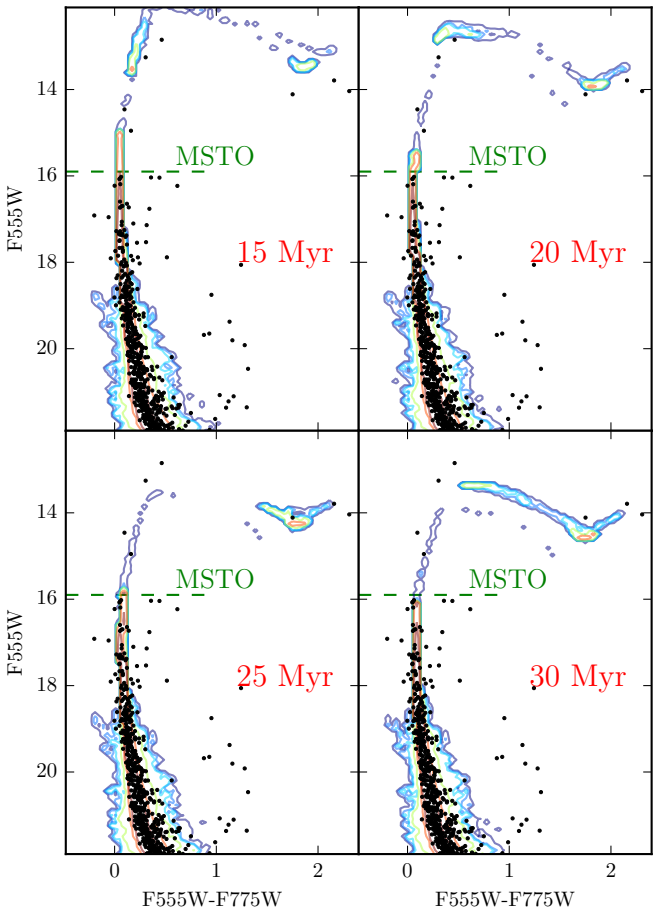

Figure 13. The same as in Fig. 7, but the synthetic CMDs are computed for Z=0.005 instead of Z=0.008.